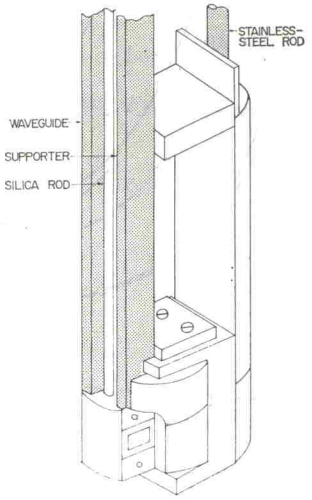

Fig. 1. Outer view of the squeezer head.

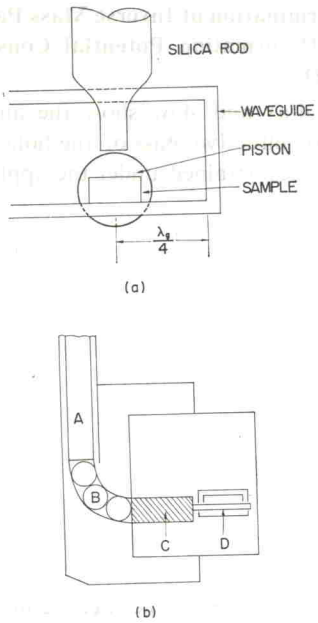

Fig. 2(a). Alignment of the piston, sample and silica rod at the central part of the parallel squeezer.
(b). Local details of the mechanism of the squeezer.

A: Pushing rod
B: Stainless-steel balls
C: Piston (shaded part)
D: Sample through the waveguide

the linewidth.[17,20,21] Samples employed are ultra-high pure germanium (70 ohm-cm) kindly supplied by Dr. H. Yonemitsu at the Tokyo Shibaura Electric Company. Balanced bridge non-resonant superheterodyne spectrometers operating at 35 GHz and 70 GHz have been used. These simplified detection systems make it possible to operate at less than 10^{-7} watt with quite a tolerable signal-to-noise ratio. Carriers are generated by white light illumination from an 8V–50W projecter lamp and through a Toshiba infrared glass filter IRD–1A, which is to cut the wavelength less than 0.9μ off.

The light intensity is weakened by operating the lamp at 1.5∼4V and using an optical iris to avoid the broadening due to carrier-carrier interactions.[22] The sample is directly immersed in the liquid helium bath.

A typical feature of the absorption lines is shown in Fig. 3.

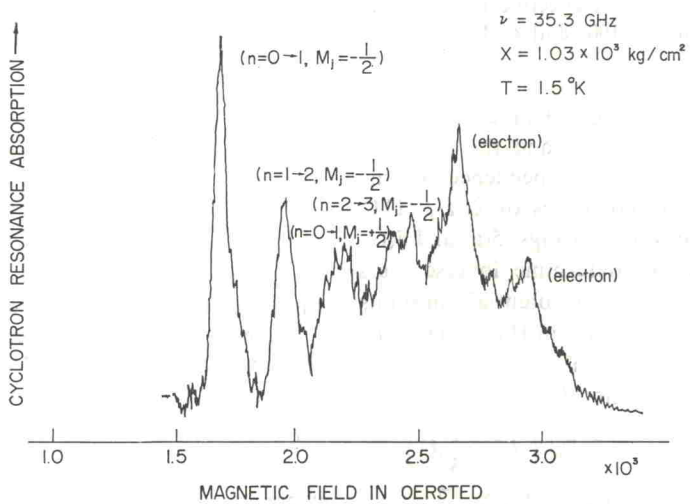

Fig. 3. A typical quantum spectrum for H, $\chi//\langle 111\rangle$.

§ 3. Determination of Inverse Mass Parameters and Deformation Potential Constants D_u and $D_{u'}$

Figures 4(a) and 4(b) show the angular dependence of effective mass of the hole cyclotron resonance lines obtained under the application of high stress, where the angle θ taken along the abscissa is between the stress and the magnetic field directions. The stress dependences of the effective mass in the geometries of χ, $H//\langle 111\rangle$ and χ, $H//\langle 100\rangle$ are shown in Figs. 5(a) and 5(b), respectively. One can determine inverse mass parameters and deformation potential constants from the above data. The strain Hamiltonian H_ε constructed by Kleiner-Roth[23] in terms of the angular momentum operator J is

$$H_\varepsilon = D_d^{\Gamma}(e_{xx}+e_{yy}+e_{zz}) + \frac{2}{3}D_u\left[\left(J_x^2-\frac{1}{3}J^2\right)e_{xx} + \left(J_y^2-\frac{1}{3}J^2\right)e_{yy} + \left(J_z^2-\frac{1}{3}J^2\right)e_{zz}\right] + \frac{2}{3}D_{u'}[\{J_xJ_y\}e_{xy}+\{J_yJ_z\}e_{yz}+\{J_xJ_z\}e_{zz}]\ ; \quad (3.1)$$

where $e_{xx}, \cdots, e_{xy}, \cdots$ are strain components while D_d^{Γ}, D_u and $D_{u'}$ are the valence band de-

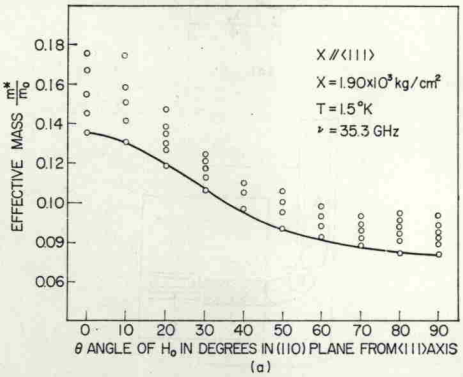

Fig. 4(a). Anisotropy of the effective mass for the hole resonance with $\chi//\langle 111\rangle$ and $\chi=1.9\times10^3$ kg/cm².

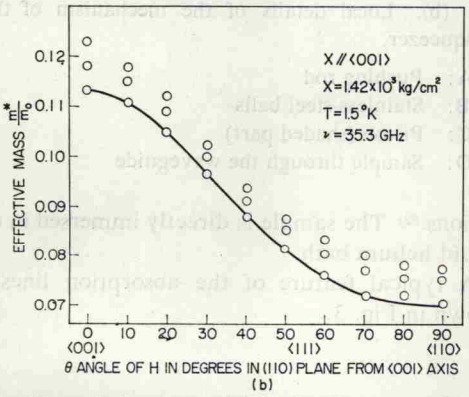

Fig. 4(b). Anisotropy of the effective mass of the hole resonance with $\chi//\langle 100\rangle$ and $\chi=1.42\times10^3$ kg/cm².

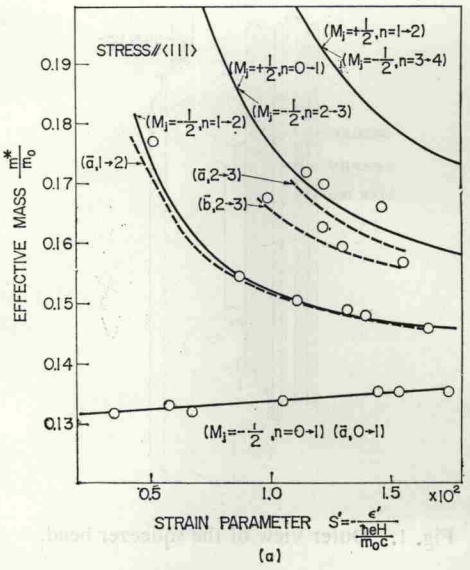

Fig. 5(a). Dependence of the effective mass of the hole cyclotron resonance lines on strain parameter[12] s' for χ, $H//\langle 111\rangle$ and 35 GHz at 1.5°K. The solid and dashed curves refer to the theoretical calculations given by the second order perturbation and by matrix diagonalization, respectively.

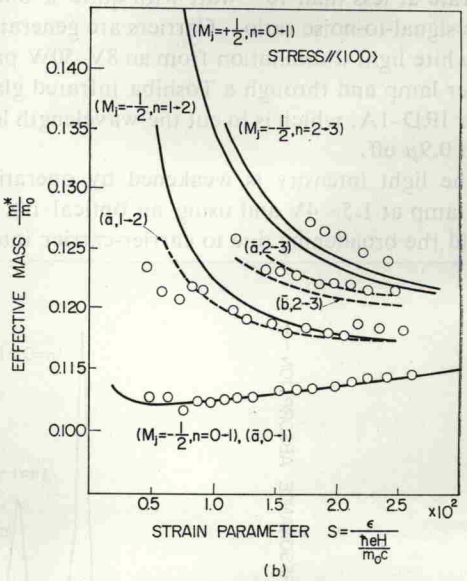

Fig. 5(b). Dependence of the effective mass of the hole cyclotron resonance lines on strain parameter s for χ, $H//\langle 100\rangle$ and 35 GHz at 1.5°K.